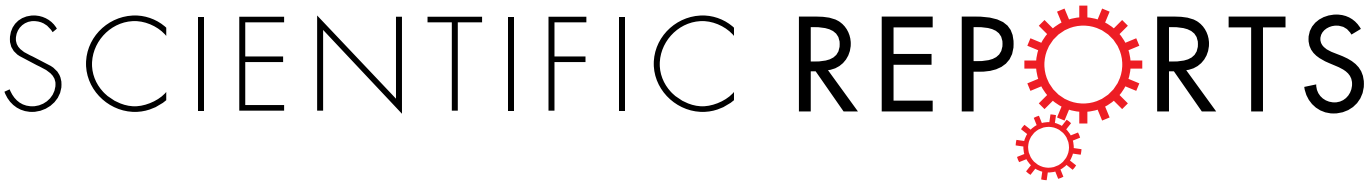

OPEN

Received: 12 October 2016
Accepted: 16 December 2016
Published: 20 January 2017

Bi-axial grown amorphous MoS_x bridged with oxygen on r-GO as a superior stable and efficient nonprecious catalyst for hydrogen evolution

Cheol-Ho Lee[1,2,*], Jin-Mun Yun[3,*], Sungho Lee[1], Seong Mu Jo[1], KwangSup Eom[4], Doh C. Lee[2], Han-Ik Joh[1] & Thomas F. Fuller[5]

Amorphous molybdenum sulfide (MoS_x) is covalently anchored to reduced graphene oxide (r-GO) via a simple one-pot reaction, thereby inducing the reduction of GO and simultaneous doping of heteroatoms on the GO. The oxygen atoms form a bridged between MoS_x and GO and play a crucial role in the fine dispersion of the MoS_x particles, control of planar MoS_x growth, and increase of exposed active sulfur sites. This bridging leads to highly efficient (−157 mV overpotential and 41 mV/decade Tafel slope) and stable (95% versus initial activity after 1000 cycles) electrocatalyst for hydrogen evolution.

Hydrogen is becoming increasingly essential as an environmentally friendly energy carrier. Global warming and abnormal climate resulting from the anthropogenic use of petroleum and environmental pollution accelerated its importance. Hence, hydrogen should be produced renewably, using clean technologies rather than by the steam reforming of natural gas. Among the potential technologies, sustainable hydrogen production using an electrochemically driven water dissociation process has been intensively explored. Efficient catalysts for the electrochemical hydrogen evolution reaction (HER) are needed to reduce the overpotential and increase the efficiency of hydrogen production. Platinum (Pt) shows the best electrocatalytic activity for the HER in acidic media; however, Pt is too expensive to be used beyond a few specialized applications. Hence, replacing Pt with low-cost and earth abundant materials for electrocatalysts is a critical challenge[1]. In-depth research seeking highly efficient and stable HER catalysts has become necessary, though various materials such as metal dichalcogenides, polymer-based carbon nitride, transition metal carbides, and nickel alloys have been proposed as promising catalysts[2–5].

Recently, a family of two-dimensional transition metal disulfides (TMDs) with MS_2 structure, where M is a transition metal such as molybdenum (Mo) or tungsten (W) and S is sulfur, has attracted much attention. These materials are a promising class of HER catalyst because they are one of the most efficient materials among the nonprecious catalysts. It is well known that the efficient electrochemical activity of the TMD stems from the S-terminated edge or strained metallic phase of MS_2, while the basal plane of semiconducting MS_2 is catalytically inert[6–8]. Jaramillo *et al.* reported that only one in four atoms of MoS_2 edge sites could evolve H_2 molecules because of the atomic hydrogen coverage of only 25% on the edge in contrast to Pt (111) as calculated by Density Functional Theory[9]. Hence, it is necessary either to synthesize nano-sized particles or to tune the electronic

[1]Carbon Convergence Materials Research Center, Institute of Advanced Composite Materials, Korea Institute of Science and Technology (KIST), chudong-ro 92, Bongdong-eup, Wanju, Jeollabukdo 55324, Republic of Korea. [2]Department of Chemical and Biomolecular Engineering (BK21+ Program), KAIST Institute for the Nanocentury, Korea Advanced Institute of Science and Technology (KAIST), Daejeon 34141, Republic of Korea. [3]Radiation Research Division for Industry and Environment, Korea Atomic Energy Research Institute (KAERI), Geumgu-gil 29, Jeongeup-si, Jeollabuk-do 56212, Republic of Korea. [4]Department of Materials Science and Engineering, Gwangju Institute of Science and Technology (GIST), Gwangju, 61005, Republic of Korea. [5]School of Chemical & Biomolecular Engineering, Georgia Institute of Technology, Atlanta, Georgia 30332, USA. *These authors contributed equally to this work. Correspondence and requests for materials should be addressed to D.C.L. (email: dclee@kaist.edu) or H.-I.J. (email: hijoh@kist.re.kr)

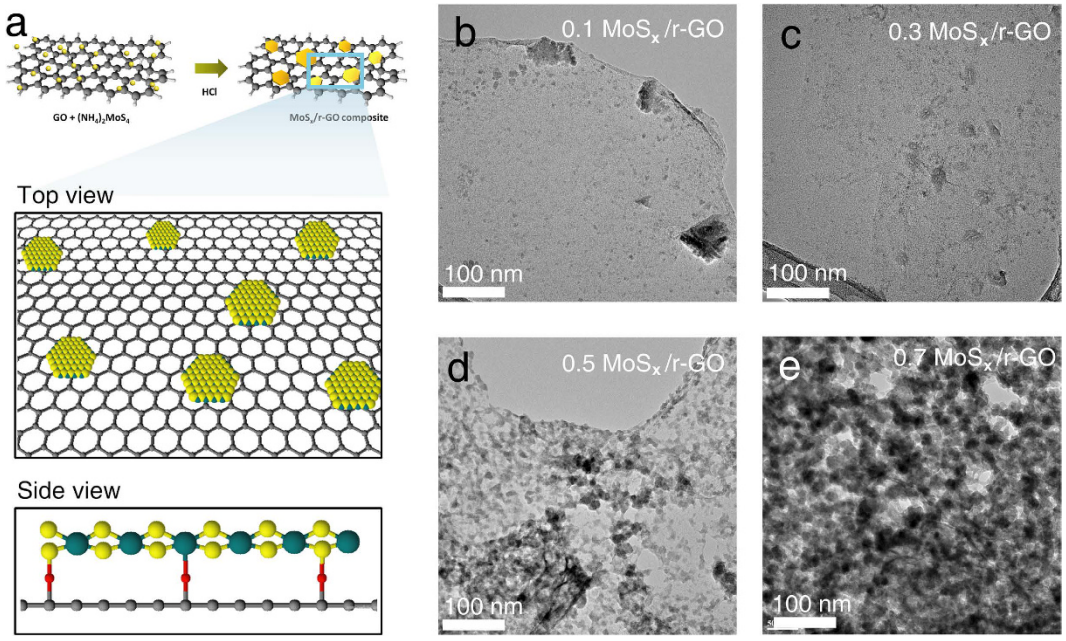

Figure 1. Synthesis of MoS_x/r-GO composites. (**a**) Schematic synthesis process and internal structure of MoS_x/r-GO at the top and side position. (**b**–**e**) TEM images of MoS_x/r-GO composites by added amount of $(NH_4)_2MoS_4$ precursor: (**b**) 0.1, (**c**) 0.3, (**d**) 0.5, and (**e**) 0.7 g.

structure of the edges to improve the activity. However, unsupported nanoscale MoS_2 with a large number of edge sites is thermodynamically unstable, leading to aggregation or transformation of the nanoparticles[10]. In addition, S-terminated edges are easily oxidized in acidic media[11]. These intrinsic properties induce the deactivation and instability of the materials when used for HER. There are two strategies to overcome these challenges: (1) controlling the morphology and (2) designing hybrid structure. Specific morphology control has been achieved using hard or soft templates such as MoO_3/MoS_2 (core/shell) nanowire, highly ordered double-gyroid MoS_2, vertically aligned MoS_2, and MoS_2 flowers[12–15]. Although these methods could prevent the degradation of MoS_2 electrochemical activity, the synthetic processes are unsuitable for the industrial scale because of their complexity and expense. Meanwhile, the hybrid structure consists of carbon supported MoS_2, which has exhibited a strong interaction between the TMD and the carbon support, minimizing the thermodynamically unstable properties and improving the morphological and electrochemical stability. However, much remains to be studied regarding the origins of the interaction and the properties of the carbon supported amorphous molybdenum sulfide. Herein, we report a one-pot synthetic strategy to produce the highly-stable and efficient MoS_x/r-GO catalyst via oxygen bridging between amorphous MoS_x and r-GO. These features are induced by the functional coupling of oxygen bridges between molybdenum sulfide and graphene oxide as shown in Fig. 1a.

Results

The molybdenum sulfide catalysts were easily synthesized by the wet-chemical reaction of $(NH_4)_2MoS_4$ and HCl in an aqueous dispersion of graphene oxide (GO) at room-temperature. The precursor was reduced to molybdenum sulfide (MoS_x, sulfur content (x) changed from 1 to 3) on the graphene supports. To investigate the effects of the amount of deposited MoS_x particles on electrochemical hydrogen production, we synthesized the MoS_x/r-GO catalysts with the amount of MoS_x precursor varying from 0.1 to 0.7 g. (Hereafter, a catalyst prepared using y g of MoS_x precursor and a fixed amount of GO is denoted as y MoS_x/r-GO sample.) For comparison, unsupported MoS_3 particles were also prepared in the absence of GO using the same process.

High-resolution transmission electron microscopy (HR-TEM) images show that both the size and the amount of MoS_x particles on thin graphene flake depend strongly on the weight of precursor used as shown in Fig. 1b–e. For 0.5 MoS_x/r-GO, the particles are uniformly deposited on the GO surface with full coverage, whereas catalysts synthesized with either less or more than 0.5 MoS_x/r-GO exhibited insufficient or aggregated particle features, respectively. However, the particle size of MoS_x/r-GO is relatively smaller than for unsupported MoS_3 (see Supplementary Figure S1). Elemental mapping was conducted using energy dispersive spectroscopy (EDS) to confirm the origin of the particles deposited on the r-GO sheets. For all MoS_x/r-GO composite samples, the positions of Mo atoms are highly correlated with the positions of S atoms, and MoS_x particles are considered to have been successfully synthesized on the r-GO sheets (see Supplementary Figure S2).

We further investigated the morphological features of as-synthesized MoS_x/r-GO composites using atomic force microscopy (AFM) as shown in Fig. 2. Each GO sheet has a thickness of ~1.1 nm consistent with double- or triple-layered GO. Similar to the TEM results for the MoS_x/r-GO composites, the width and height of MoS_x on the r-GO composites depend on the amount of MoS_x precursor. The average width of the MoS_x particles on r-GO were increased from 50.2 nm to 58.8, 66.8, and 87.6 nm for 0.1, 0.3, 0.5, and 0.7 MoS_x/r-GO, respectively. Average

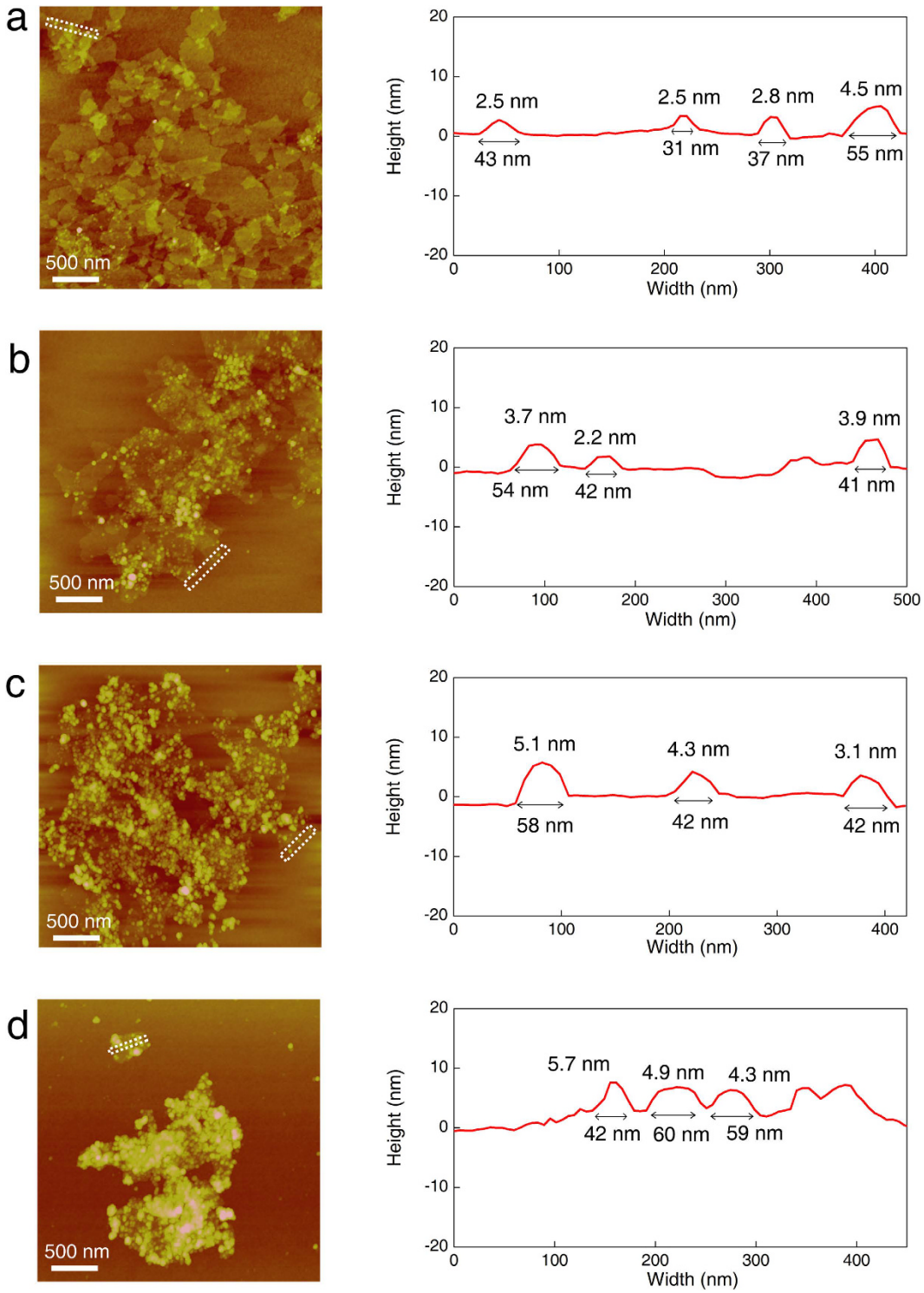

Figure 2. AFM images of as-synthesized MoS_x/r-GO composites by added amount of $(NH_4)_2MoS_4$ precursor. (**a**) 0.1, (**b**) 0.3, (**c**) 0.5, and (**d**) 0.7 g, and corresponding height spectra along with dashed rectangles in AFM images indicating that MoS_x on r-GO has a planar shape with a high aspect ratio.

thickness also gradually increased from 2.9 nm to 4.3, 5.6, and 7.7 nm for 0.1, 0.3, 0.5, and 0.7 MoS_x/r-GO respectively. The unsupported MoS_3 particles synthesized using the same method show a larger average particle width of 117.8 nm and height of 22.3 nm (see Supplementary Figure S3). Interestingly, all the MoS_x/r-GO composites show a very high aspect ratio–above 10, in contrast to the unsupported MoS_3. This result indicates that MoS_x particles were biaxially grown on the r-GO surface in a planar or coin shape. Thus, we believed that interaction between the precursor and the GO might affect the growth and morphology of the particles, which are closely related to the catalytically active edge sites[16].

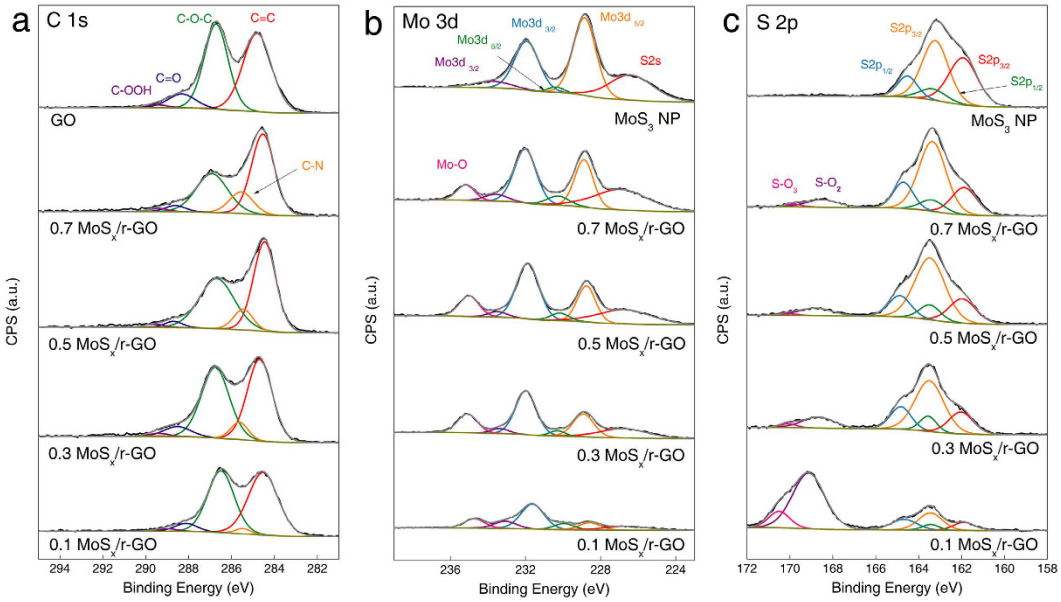

Figure 3. XPS spectra and fitted peaks of MoS_x/r-GO composites. (**a**) C1s spectra shows reduction of GO with increasing precursor. (**b**) Fitted Mo3d peaks indicate Mo with both 4+ and 5+ oxidation states. (**c**) Deconvolution of S2p consisting of both terminal S and bridging S.

The structural composition and interaction between the MoS_x and r-GO were investigated using X-ray photoelectron spectroscopy (XPS) as shown in Fig. 3. The XPS spectra of all composite samples exhibited predominant C1s, Mo3d, and S2p peaks. The peak intensities of oxygen functional groups on the GO, such as epoxy, carbonyl, and carboxyl groups, which are observed at binding energies (BE) of 286.7, 288.4, and 289.5 eV, respectively, gradually decreased with increasing precursor concentrations (Fig. 3a). Thus, it is believed that the insulating GO substrate can be spontaneously reduced to the conductive r-GO by the hydrazine or ammonium chloride species generated during the growth reaction of MoS_x particles[17]. Similar trends were observed in the X-ray diffraction (XRD) patterns of the GO and MoS_x/r-GO composites as shown in Figure S4. The sharp (001) peak of GO at 10.8 degrees, which represents the wider interlayer distance between the graphitic layers compared to graphite, was shifted into the (002) plane at 22.0 degrees for the composites.

Remarkably, the stoichiometric S/Mo ratios of the composite gradually increased from 1.5 to 2.3, 2.6, and 3.3 for 0.1, 0.3, 0.5, and 0.7 MoS_x/r-GO, respectively, while the ratio of unsupported MoS_3 particles was approximately ~3.0, indicating the MoS_3 structure. The Mo 3d spectrum with Mo $3d^{3/2}$ and Mo $3d^{5/2}$ doublets indicates that the Mo metal in all composite samples had the 4+ oxidation state. In particular, $Mo3d^{3/2}$ (233.2 eV) and $Mo3d^{5/2}$ (230.0 eV) in the composite samples were observed at higher BE than in unsupported MoS_3 (231.5 eV and 228.4 eV for $Mo3d^{3/2}$ and $Mo3d^{5/2}$, respectively). These values can be attributed to the presence of Mo^{5+} and indicate that each of the Mo atoms in the composites was randomly bonded with 2 ~ 3S atoms as indicated in the stoichiometric S/Mo ratio. Wang *et al.* reported that MoS_x was a fundamentally and thermodynamically amorphous structure with many active edge sites, in contrast to crystalline MoS_2, when the stoichiometric ratio of S atoms to Mo atoms is above 2[18]. There are broad diffraction peaks in all our MoS_x and MoS_3 particles in XRD patterns of Figure S4. Thus, the resulting MoS_x particles have an amorphous structure irrespective of the GO, which is expected to expose more active edge sites of MoS_x.

The S 2p spectrum consists of two doublets. One doublet with higher BE ($S2p^{3/2}$ = 163.2 eV and $S2p^{1/2}$ = 164.6 eV) is attributed to the existence of both bridging S_2^{2-} and/or apical S^{2-} ligands. The other doublet with relatively lower BE ($S2p^{3/2}$ = 162.0 eV and $S2p^{1/2}$ = 163.2 eV) stems from the existence of the terminal S_2^{2-} and/or S^{2-} [19]. Considering the previous reports that the HER activity of MoS_x is highly correlated to the amount of terminated S-edge sites, it can be expected that the abundance of catalytic edge sites estimated from the deconvolution of S peaks (area ratio of edged versus bridged S = ~5/4) has a beneficial effect on the hydrogen evolution efficiency.

Importantly, new peaks related to molybdenum-oxygen (Mo-O) bonding (235.6 eV) and sulfur-oxygen (S-O) bonding (169.2 and 170.5 eV) are observed only for the MoS_x/r-GO composite in the presence of graphene oxide. The amount of S-O bonding, both the strong SO_2 and weak SO_3 configurations, significantly decreases with increasing precursor concentration, while Mo-O bonding (MoO) increases slightly with precursor concentration. In particular, in the case of 0.5 MoS_x/r-GO, 12.4 and 7.3 atomic percent of the molybdenum and sulfur atoms, respectively, in the edge area of MoS_x particles are covalently bonded to oxygen functional groups on r-GO sheets[20]. Therefore, we believe that most of the epoxide among the oxygen functional groups plays a crucial role in the anchoring or bridging between MoS_x and GO. From the XPS analysis, we can conclude that the novel oxygen-bridged structure could induce the modulation of particle growth, Mo/S stoichiometry, and an amorphous configuration with more exposed active sites, which are expected to improve catalytic activity for hydrogen evolution.

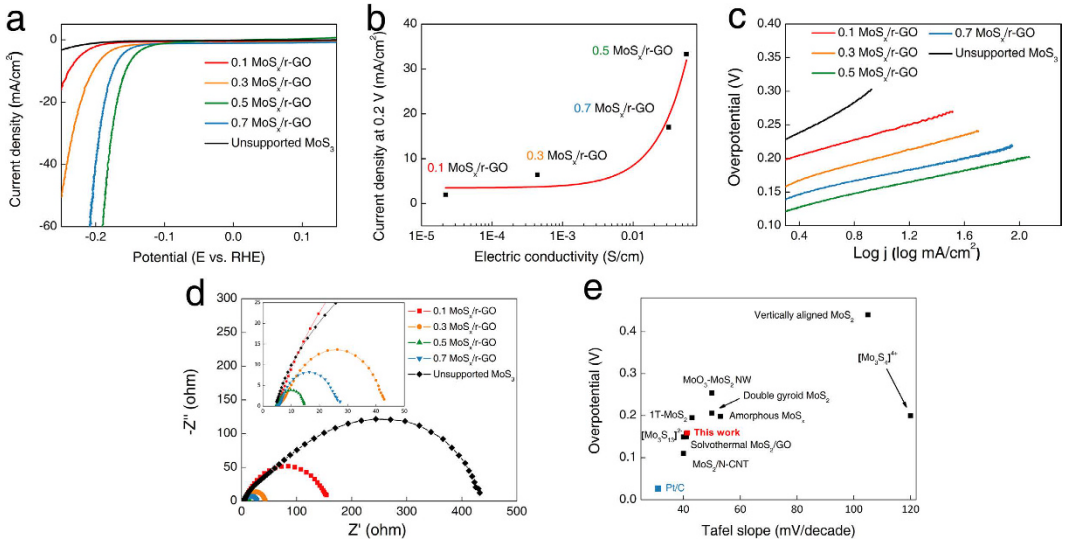

Figure 4. (**a**) Polarized curves of each MoS_x/r-GO catalysts and unsupported MoS_3, (**b**) relationship between electrical conductivity and HER activity. (**c**) The corresponding Tafel plot obtained from polarized curve. (**d**) Nyquist plots measured at 0.2 V. (**e**) Overpotential and Tafel slope of various molybdenum sulfide catalysts.

We investigated the electrochemical HER performance of MoS_x/r-GO composites deposited on a glassy carbon electrode in 0.5 M H_2SO_4 aqueous electrolyte using a typical three electrode setup as shown in the polarization curves (J-V) of current density (J) plotted against potential (V) of Fig. 4a. The overpotentials of all MoS_x/r-GO composites at 10 mA/cm^2 were −240, −204, −157, and −176 mV for 0.1, 0.3, 0.5, and 0.7 MoS_x/r-GO respectively. The activity of composite catalysts in the precursor range from 0.1 to 0.5 g dramatically improved from J = −1.5 to −59.7 mA/cm^2 at 190 mV (vs RHE). On the other hand, the HER activity of the 0.7 MoS_x/r-GO catalyst was comparatively decreased, probably due to decreased electrical conductivity and reduced catalytically active sites[21]. The conductivity of 0.5 MoS_x/r-GO (5.7×10^{-2} S/cm) measured by the 4-point probe resistivity measurement was three and two orders higher in magnitude than the conductivity of 0.1 and 0.3 MoS_x/r-GO, respectively. The increased conductivity would be originated from the reduction of GO. At the same time, 0.7 MoS_x/r-GO had a 44% lower value of 3.2×10^{-2} S/cm, with respect to the relatively low amount of r-GO even though the high degree of reduction. Therefore, we concluded that the current density for the HER is closely related to the conductivity as shown in Fig. 4b; and thus high electrical conductivity would mainly affect the improvement of electrochemical HER activity.

To confirm the quantitative catalytic activity and rate determining step (RDS), we fitted a Tafel plot based on the HER polarization curves as shown in Fig. 4c. The calculated Tafel slopes were 54, 53, 42, 41, and 112 mV/decade for 0.1, 0.3, 0.5, 0.7 MoS_x/r-GO, and unsupported MoS_x particles, respectively. The possible HER process in acidic electrolyte generally consists of three steps; Volmer ($H^+ + e^- \rightarrow H_{ads}$, <120 mV/decade), Heyrovsky ($H_{ads} + h^+ + e^- \rightarrow H_2$, <40 mV/decade), and Tafel ($H_{ads} + H_{ads} \rightarrow H_2$, <30 mV/decade)[22]. Considering the Tafel slopes of the catalysts, both the unsupported MoS_x and the MoS_x/r-GO in this study might favor an electrochemical desorption mechanism, in which electrochemical desorption is the RDS, although the inherent mechanism of Mo sulfide based catalysts has been inconclusive to date[16]. However, the resulting Tafel slope of 0.5 MoS_x/r-GO is the smallest among the catalysts. Previous studies have reported that the major factors affecting the HER activity are the surface energy for hydrogen desorption and the rate of electron transfer[23]. It is well-known that MoS_x itself is a semiconducting material, while the surface energy of MoS_x is theoretically limited to desorbing the hydrogen[23]. Thus, it can be concluded that obvious differences in the HER activity of the catalysts attributed to the electron transfer are evident in the electrochemical impedance spectra at 0.2 V (vs RHE). The MoS_x/r-GO catalysts, especially 0.5(~14.6 Ω), show far lower charge-transfer impedance than unsupported MoS_x (~432.6 Ω), leading to higher HER activity (Fig. 4d). In addition, calculated active site and turnover frequency (TOF) of 0.5 MoS_x/r-GO at 0.1 V were 2.11 * 10^{14} Mo atoms/cm^2 and 4.8 s^{-1}, respectively. The values of MoS_x/r-GO are similar value compared to other studies[19,24]. The resulting overpotential and Tafel slope of 0.5 MoS_x/r-GO are among of the best values among the recently published studies on materials such as highly conductive molybdenum sulfides (1T-MoS_2, MoS_x/N-CNT, solvothermal MoS_2, and $[Mo_3S_{13}]^{2-}$) and conventional molybdenum sulfides with no conductive substrate (double gyroid MoS_2, vertically aligned MoS_2, MoO_3-MoS_2 nanowire (NW), amorphous MoS_x, and $[Mo_3S_4]^{4-}$) as shown in Fig. 4e[12–14,16,19,25–28]. The achieved performance for hydrogen production is significantly useful compared to the materials for solar hydrogen production[29,30].

The catalytic stability of 0.5 MoS_x/r-GO over 3,000 cycles was measured by cyclic voltammetry with a potential range from −0.3 to 0.2 V as shown in Fig. 5a. After 3,000 cycles, there is no significant change in HER performance except for a slight potential shift. Kibsgaard reported that the slight potential shift caused by not the decline of electrocatalytic activity but rigorous H_2 bubble formation in structure of electrodes, which ultimately results in fewer active sites for HER[19]. In contrast, unsupported MoS_x showed a considerable decrease in current

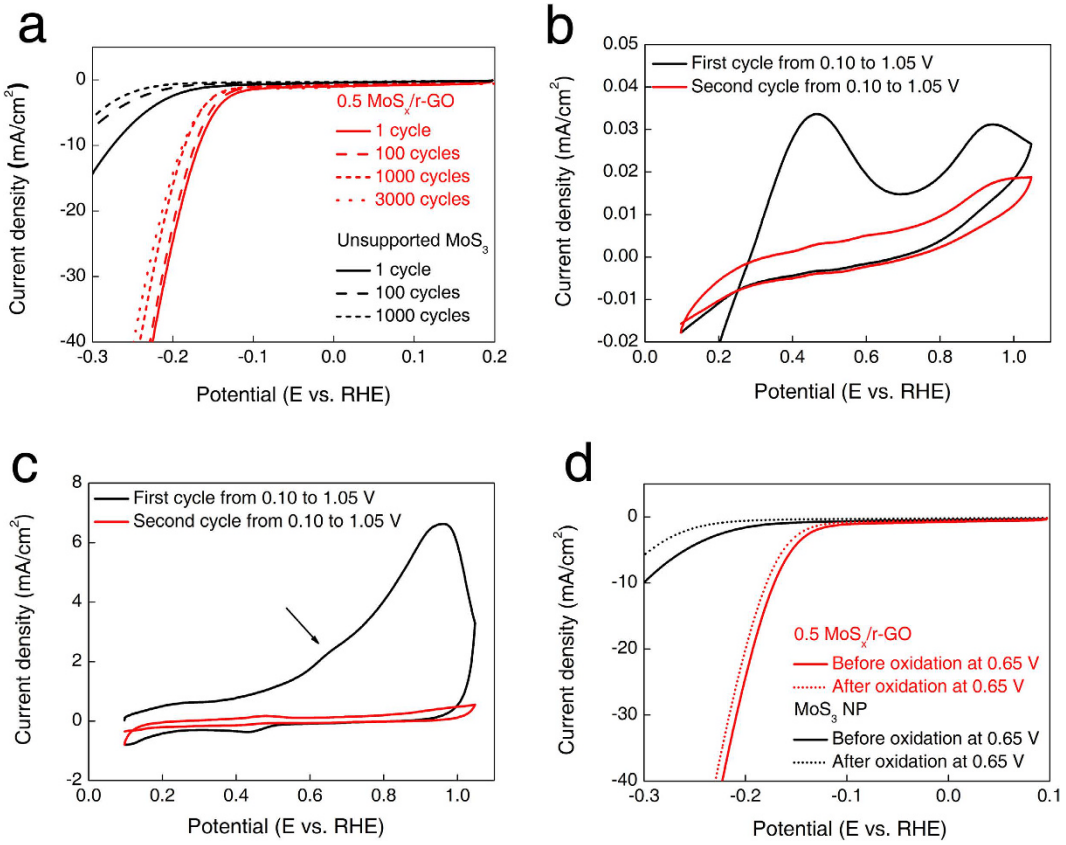

Figure 5. (**a**) Catalytic stability of 0.5 MoS_x/r-GO composite for 3,000 cycles and unsupported MoS_3 for 1,000 cycles. Cyclic voltammetry of (**b**) unsupported MoS_3 and (**c**) 0.5 MoS_x/r-GO from 0.10 to 1.05 V. (**d**) HER activity of unsupported MoS_3 and 0.5 MoS_x/r-GO before/after electrochemical oxidation at 0.65 V.

density from 14.5 to 5.6 mA/cm^2 after 1,000 cycles. It is believed that the excellent durability of MoS_x/r-GO originated from the functional coupling of oxygen bridges between MoS_x and r-GO, leading to thermodynamic stability of the MoS_x particles. The XPS analysis was conducted to investigate the structural changes before and after the durability test. The atomic ratio of S to Mo after the durability test was converted from 2.6 to 2.0 based on the XPS spectrum as shown in Figure S6. Further, the BE of the deconvoluted S 2p peaks was also shifted to lower positions, as in MoS_2. Previous studies reported that MoS_3 is electrochemically reduced to MoS_2 as the active species for HER[31]. However, covalent S-O and Mo-O bonds are retained after 1,000 cycles, indicating that MoS_x particles could be anchored on the r-GO. Therefore, we believe that the oxygen bridges might improve the stability of HER compared to MoS_3 on multi walled carbon nanotubes with no functional coupling between the MoS_3 and the support (88% after 500 cycles vs initial activity)[32].

The functional coupling between MoS_x and r-GO was also significantly effective in preventing oxidation from affecting catalytic stability. The electrochemical oxidation test was conducted in 0.5 M H_2SO_4 electrolyte at positive potential. Unsupported MoS_3 initially shows two dominant oxidation peaks at approximately 0.50 and 0.95 V as depicted in Fig. 5b. Thermodynamically unstable sulfur atoms located at edge sites are oxidized first at 0.5 V, and the rest of sulfur atoms in the basal plane are then oxidized later at nearly 0.95 V[33]. However, the oxidation potential of 0.5 MoS_x/r-GO is positively shifted to 0.65 V (black arrow in Fig. 5c), indicating high oxidation resistance that is closely related to the stability. In addition, after electrochemical oxidation at 0.65 V, 0.5 MoS_x/r-GO exhibits a negligible potential shift, whereas the current density of unsupported MoS_x decreases significantly as shown in Fig. 5d. Therefore, the novel functional coupling of oxygen could induce anchoring and oxidation-resistance effects through the strong interaction between MoS_x and r-GO, leading to the realization of Mo sulfide based catalysts with tremendous activity and durability.

Discussion

In summary, we synthesized MoS_x anchored r-GO composite catalysts by a simple one-pot solution process at room temperature. MoS_x particles were covalently bonded to r-GO through oxygen functional groups, and GO was simultaneously reduced to conductive r-GO. The oxygen atoms bridged between MoS_x and GO play substantial roles in the fine dispersion of MoS_x particles, control of planar MoS_x growth, and increase of exposed active sulfur sites, leading to highly efficient and stable electrocatalysts for hydrogen evolution. Therefore, biaxially grown MoS_x anchored with r-GO could act as promising nonprecious electrocatalysts for the future hydrogen-based energy world.

Methods

The preparation of GO. The GO was prepared via a modified Hummers method as described in a previous report[16]. First, graphite was dispersed in sulfuric acid (133 mg/ml) by sonication and stirring. Then, $KMnO_4$ was slowly added to suspension at low temperature, which was kept at 45 °C for 6 h. Then, 100 mL of distilled water and 20 mL of H_2O_2 were added to remove any residual oxidizing agent. The brownish mixture was washed by centrifugation. The resulting gel-like GO was freeze-dried at −45 °C for 24 h and used for the preparation of the MoS_x/r-GO composite materials.

The preparation of MoS_x/r-GO composite materials. First, GO was dispersed in deionized water at a concentration of 3 mg/ml with a brief bath-sonication. Then, a specific amount of ammonium thiomolybdate (0.1, 0.3, 0.5, or 0.7 g) as a MoS_x precursor was separately added in 100 ml of GO dispersion with constant stirring at room temperature. Hydrochloric acid (5 ml) was slowly added to the homogeneous mixture. After gas evolution was completed, the product was centrifuged at 7000 rpm for 10 min, followed by washed using ethanol and water to remove acidic residues. Finally, the resulting gel-like MoS_x/r-GO was freeze-dried at −45 °C for 24 h and used as the hydrogen evolution catalyst.

Sample characterization. The crystal structure was investigated using XRD equipment (Smartlab 3, Rigaku) with a scan rate of 2 degree/min from 5 to 70 degrees. The morphologies of the prepared materials were analyzed using atomic force microscopy (AFM, Veeco, Digital Instruments Nanoscope IIIA). A sample for AFM measurement was prepared by spin-coating the catalyst dispersed in DMF at a concentration of ~1 mg/mL onto a Si wafer. The surface morphology and atomic contents of Mo, S, and C in the catalysts were analyzed using a field emission transmission electron microscope (FETEM, JEOL, JEM-2200FS) and X-ray photoelectron spectroscopy (XPS, Thermo Fisher, Multilab 2000), respectively. The TEM specimens were prepared by mixing the products in ethanol using an ultrasonic bath for 5 min, and then a drop of the suspension was placed on a copper grid. The XPS data were recorded using Al Kα radiation ($h\nu = 1000$ eV). The electrical conductivity was investigated using a four-point probe instrument (FPP-RS8, Dasol Eng.) and the film thickness of each catalyst was analyzed using a surface profiler (Alphastep IQ, KLA Tencor).

Electrochemical analysis. First, 15 mg of each MoS_x/r-GO composite powder was dispersed in a mixture of 1000 μl of DMF and 100 μL of Nafion with a brief sonication. Then, 8 μL of the prepared sample was deposited on glassy carbon electrode stand tried at at 50 °C. Linear sweep voltammetry using a potentiostat with a scan rate of 5 mVs^{-1} was conducted in 0.5 M H_2SO_4 electrolyte using an Ag/AgCl electrode as the reference electrode and a platinum wire as the counter electrode.

Calculation of electrochemical active sites and TOF. The oxidation peak at lower potential indicated the oxidation potential of edge area of MoS_x to MoO_2 as shown in Fig. 5c. Thus, total current of edge oxidation peak was used to calculate the electrochemical active sites. The following equations were used to calculate the active sites and TOF.

$$\begin{aligned}\text{Total hydrogen turnover} &= (\text{current density, A/cm}^2)/(96485.3\,\text{C/mol e}^-)\\ &\quad /(2\ \text{mol e}^-/\text{H}_2) * (6.022 * 10^{23}\ \text{molecules of H}_2/1\,\text{mol H}_2)\end{aligned} \tag{1}$$

$$\begin{aligned}\text{Electrochemical active sites} &= (\text{area of edge oxidation peak, C/cm}^2)\\ &\quad * (6.24 * 10^{18}\ \text{electrons})/(8.9\ \text{electrons/Mo})\end{aligned} \tag{2}$$

$$\text{TOF} = (\text{total hydrogen turnover})/(\text{electrochemical active sites}) \tag{3}$$

we assumed that the average number of electrons for each Mo oxidation is approximately 8.9 electrons[32].

References

1. Sheng, W., Gasteiger, H. A. & Shao-Horn, Y. Hydrogen Oxidation and Evolution Reaction Kinetics on Platinum: Acid vs Alkaline Electrolytes. *J. Electrochem. Soc.* **157,** B1529–B1536, doi: 10.1149/1.3483106 (2010).
2. Yang, F. *et al.* Solar hydrogen evolution using metal-free photocatalytic polymeric carbon nitride/CuInS2 composites as photocathodes. *J. Mater. Chem. A* **1,** 6407–6415, doi: 10.1039/c3ta10360a (2013).
3. Gong, M. *et al.* Nanoscale nickel oxide/nickel heterostructures for active hydrogen evolution electrocatalysis. *Nat. Commun.* **5,** doi: 10.1038/ncomms5695 (2014).
4. Chung, D. Y. *et al.* Edge-exposed MoS2 nano-assembled structures as efficient electrocatalysts for hydrogen evolution reaction. *Nanoscale* **6,** 2131–2136, doi: 10.1039/c3nr05228a (2014).
5. Lukowski, M. A. *et al.* Highly active hydrogen evolution catalysis from metallic WS2 nanosheets. *Energy Environ. Sci.* **7,** 2608–2613, doi: 10.1039/c4ee01329h (2014).
6. Tsai, C., Abild-Pedersen, F. & Nørskov, J. K. Tuning the MoS2 Edge-Site Activity for Hydrogen Evolution via Support Interactions. *Nano Lett.* **14,** 1381–1387, doi: 10.1021/nl404444k (2014).
7. Tsai, C., Chan, K., Abild-Pedersen, F. & Norskov, J. K. Active edge sites in MoSe2 and WSe2 catalysts for the hydrogen evolution reaction: a density functional study. *Phys. Chem. Chem. Phys.* **16,** 13156–13164, doi: 10.1039/c4cp01237b (2014).
8. Lin, J. *et al.* Enhanced Electrocatalysis for Hydrogen Evolution Reactions from WS2 Nanoribbons. *Adv. Energy Mater*. **4,** doi: 10.1002/aenm.201301875 (2014).
9. Jaramillo, T. F. *et al.* Identification of Active Edge Sites for Electrochemical H2 Evolution from MoS2 Nanocatalysts. *Science* **317,** 100–102, doi: 10.1126/science.1141483 (2007).
10. Albu-Yaron, A. *et al.* MoS2 Hybrid Nanostructures: From Octahedral to Quasi-Spherical Shells within Individual Nanoparticles. *Angew. Chem. Int. Ed.* **50,** 1810–1814, doi: 10.1002/anie.201006719 (2011).

11. Yun, J.-M. *et al.* Exfoliated and Partially Oxidized MoS2 Nanosheets by One-Pot Reaction for Efficient and Stable Organic Solar Cells. *Small* **10,** 2319–2324, doi: 10.1002/smll.201303648 (2014).
12. Chen, Z. *et al.* Core–shell MoO3–MoS2 Nanowires for Hydrogen Evolution: A Functional Design for Electrocatalytic Materials. *Nano Lett.* **11,** 4168–4175, doi: 10.1021/nl2020476 (2011).
13. Kibsgaard, J., Chen, Z., Reinecke, B. N. & Jaramillo, T. F. Engineering the surface structure of MoS2 to preferentially expose active edge sites for electrocatalysis. *Nat. Mater.* **11,** 963–969, doi: http://www.nature.com/nmat/journal/v11/n11/abs/nmat3439.html#supplementary-information (2012).
14. Kong, D. *et al.* Synthesis of MoS2 and MoSe2 Films with Vertically Aligned Layers. *Nano Lett.* **13,** 1341–1347, doi: 10.1021/nl400258t (2013).
15. Bhimanapati, G. R. *et al.* Growth and Tunable Surface Wettability of Vertical MoS2 Layers for Improved Hydrogen Evolution Reactions. *ACS Appl. Mater. Interfaces* 8, 22190–22195, doi: 10.1021/acsami.6b05848 (2016).
16. Li, Y. *et al.* MoS2 Nanoparticles Grown on Graphene: An Advanced Catalyst for the Hydrogen Evolution Reaction. *J. Am. Chem. Soc.* **133,** 7296–7299, doi: 10.1021/ja201269b (2011).
17. Kim, S.-H. *et al.* Fluorine-functionalized and simultaneously reduced graphene oxide as a novel hole transporting layer for highly efficient and stable organic photovoltaic cells. *Nanoscale* **6,** 7183–7187, doi: 10.1039/c4nr01038h (2014).
18. Wang, J. *et al.* Characterization of Nanosize Molybdenum Trisulfide for Lithium Batteries and MoS3 Structure Confirmation via Electrochemistry. *Electrochem. Solid-State Lett.* **10,** A204–A207, doi: 10.1149/1.2750227 (2007).
19. Kibsgaard, J., Jaramillo, T. F. & Besenbacher, F. Building an appropriate active-site motif into a hydrogen-evolution catalyst with thiomolybdate [Mo3S13]2− clusters. *Nat. Chem.* **6,** 248–253, doi: 10.1038/nchem.1853 http://www.nature.com/nchem/journal/v6/n3/abs/nchem.1853.html#supplementary-information (2014).
20. da Silveira Firmiano, E. G. *et al.* Supercapacitor Electrodes Obtained by Directly Bonding 2D MoS2 on Reduced Graphene Oxide. *Adv. Energy Mater.* **4,** doi: 10.1002/aenm.201301380 (2014).
21. Zheng, X. *et al.* Space-Confined Growth of MoS2 Nanosheets within Graphite: The Layered Hybrid of MoS2 and Graphene as an Active Catalyst for Hydrogen Evolution Reaction. *Chem. Mater.* **26,** 2344–2353, doi: 10.1021/cm500347r (2014).
22. Hinnemann, B. *et al.* Biomimetic Hydrogen Evolution: MoS2 Nanoparticles as Catalyst for Hydrogen Evolution. *J. Am. Chem. Soc.* **127,** 5308–5309, doi: 10.1021/ja0504690 (2005).
23. Benck, J. D., Hellstern, T. R., Kibsgaard, J., Chakthranont, P. & Jaramillo, T. F. Catalyzing the Hydrogen Evolution Reaction (HER) with Molybdenum Sulfide Nanomaterials. *ACS Catal.* **4,** 3957–3971, doi: 10.1021/cs500923c (2014).
24. Ma, L. *et al. In Situ* Thermal Synthesis of Inlaid Ultrathin MoS2/Graphene Nanosheets as Electrocatalysts for the Hydrogen Evolution Reaction. *Chem. Mater.* **28,** 5733–5742, doi: 10.1021/acs.chemmater.6b01980 (2016).
25. Li, D. J. *et al.* Molybdenum Sulfide/N-Doped CNT Forest Hybrid Catalysts for High-Performance Hydrogen Evolution Reaction. *Nano Lett.* **14,** 1228–1233, doi: 10.1021/nl404108a (2014).
26. Lukowski, M. A. *et al.* Enhanced Hydrogen Evolution Catalysis from Chemically Exfoliated Metallic MoS2 Nanosheets. *J. Am. Chem. Soc.* **135,** 10274–10277, doi: 10.1021/ja404523s (2013).
27. Benck, J. D., Chen, Z., Kuritzky, L. Y., Forman, A. J. & Jaramillo, T. F. Amorphous Molybdenum Sulfide Catalysts for Electrochemical Hydrogen Production: Insights into the Origin of their Catalytic Activity. *ACS Catal.* **2,** 1916–1923, doi: 10.1021/cs300451q (2012).
28. Jaramillo, T. F. *et al.* Hydrogen Evolution on Supported Incomplete Cubane-type [Mo3S4]4+ Electrocatalysts. *J. Phys. Chem. C* **112,** 17492–17498, doi: 10.1021/jp802695e (2008).
29. Weber, M. F. & Dignam, M. J. Efficiency of Splitting Water with Semiconducting Photoelectrodes. *J. Electrochem. Soc.* **131,** 1258–1265, doi: 10.1149/1.2115797 (1984).
30. Walter, M. G. *et al.* Solar Water Splitting Cells. *Chem. Rev.* **110,** 6446–6473, doi: 10.1021/cr1002326 (2010).
31. Merki, D., Fierro, S., Vrubel, H. & Hu, X. Amorphous molybdenum sulfide films as catalysts for electrochemical hydrogen production in water. *Chem. Sci.* **2,** 1262–1267, doi: 10.1039/c1sc00117e (2011).
32. Lin, T.-W., Liu, C.-J. & Lin, J.-Y. Facile synthesis of MoS3/carbon nanotube nanocomposite with high catalytic activity toward hydrogen evolution reaction. *Appl. Catal. B* **134–135,** 75–82, doi: http://dx.doi.org/10.1016/j.apcatb.2013.01.004 (2013).
33. Bonde, J., Moses, P. G., Jaramillo, T. F., Norskov, J. K. & Chorkendorff, I. Hydrogen evolution on nano-particulate transition metal sulfides. *Faraday Discuss.* **140,** 219–231, doi: 10.1039/b803857k (2009).

Acknowledgements

The authors acknowledge the financial supports of this work from the Korea Institute of Science and Technology, Republic of Korea.

Author Contributions

C.-H. Lee, J.–M. Yun and H.-I. Joh wrote the main manuscript text. C.-H. Lee, J.-M. Yun and K. S. Eom prepared and characterized all samples in this manuscript. T. F. Fuller, D. Lee and S. Lee discussed and advised the experimental results. All authors reviewed the manuscript.

Additional Information

Supplementary information accompanies this paper at http://www.nature.com/srep

Competing financial interests: The authors declare no competing financial interests.

How to cite this article: Lee, C.-H. *et al.* Bi-axial grown amorphous MoS_x bridged with oxygen on r-GO as a superior stable and efficient nonprecious catalyst for hydrogen evolution. *Sci. Rep.* **7**, 41190; doi: 10.1038/srep41190 (2017).

Publisher's note: Springer Nature remains neutral with regard to jurisdictional claims in published maps and institutional affiliations.